Silicon diffusion in AlN

V Bonito Oliva, D Mangelinck, S Hagedorn, H Bracht, K Irmscher, C Hartmann, P Vennéguès, M Albrecht

Silicon diffusion in AlN

V. Bonito Oliva[1,2*], D. Mangelinck[3], S. Hagedorn[4], H. Bracht[5], K. Irmscher[1], C. Hartmann[1], P. Vennéguès[2] and M. Albrecht[1]

[1]*Leibniz-Institut für Kristallzüchtung, Max-Born Straße 2, 12489 Berlin, Germany*
[2]*Université Côte d'Azur, CRHEA-CNRS, rue B. Grégory, 06560 Valbonne, France*
[3]*Aix Marseille Université, CNRS, IM2NP, Faculté de Saint-Jérôme, 13397 Marseille cedex 20, France*
[4]*Ferdinand-Braun-Institut (FBH), Leibniz-Institut für Höchstfrequenztechnik, Gustav-Kirchhoff-Str. 4, 12489 Berlin, Germany*
[5]*Institute of Materials Physics, University of Münster, D-48149 Münster, Germany*
*email: valeria.bonito-oliva@ikz-berlin.de

ABSTRACT

In this study, we investigate the diffusion of Si donors in AlN. Amorphous $Si_{1-x}N_x$ sputtered on the surface of bulk AlN with low dislocation density is used as a Si source. The diffusion experiments are conducted through isochronal and isothermal annealing in a protective N_2 atmosphere at temperatures between 1500°C and 1700°C. The Si depth profiles measured by secondary ion mass spectrometry exhibit a convex box-like shape with a steep diffusion front. These concentration profiles are best described with a diffusion coefficient that depends on the square of the local Si concentration. From the characteristic box-shaped Si profiles, we conclude that diffusion of Si in AlN is mediated by singly negatively charged dopant-vacancy pairs $Si_{Al}V_{Al}^{-}$. The strong concentration dependence of Si diffusion is due to the electric field associated with the incorporation of Si donors (Si_{Al}^{+1}) on substitutional Al lattice sites and reflects that Si is fully electrically active at diffusion temperature. The experimentally obtained extrinsic Si diffusion coefficient is reduced to intrinsic doping conditions. The temperature dependence of Si diffusion for intrinsic conditions is described by an activation enthalpy of (10.34 ± 0.32) eV and a pre-exponential factor $235\,^{+1485}_{-203}$ cm^2s^{-1}. The migration enthalpy of the donor-vacancy pair $Si_{Al}V_{Al}^{-}$ is estimated to be around 3.5 eV. This estimation is based on the activation enthalpy of the transport

capacity of $Si_{Al}V_{Al}^{-}$ and theoretical results concerning the formation energy of negatively charged vacancies on Al-sites in AlN.

INTRODUCTION

AlN and Al-rich $Al_xGa_{1-x}N$ are attractive candidates for deep-UV optoelectronic and high power and RF electronic devices thanks to their wide band gap, high breakdown field, high saturation velocity, high thermal conductivity and resistance to harsh environmental conditions. One of the main challenges in the development of AlN applications is to obtain efficient p-type and n-type doping. As for other wide bandgap semiconductors, effective doping is challenged by the low formation energies of compensating defects or DX centers, as described by the "doping limiting rule" [1]. In Al-rich $Al_xGa_{1-x}N$, doping above a critical Si concentration leads to a decrease of the free electron concentration and presents a severe limitation for the development of applications [2]. It has been hypothesized that Si may form DX centers beyond a critical Al composition and doping concentration [3] [4] [5]. In AlN, n-type doping is realized by incorporation of e.g. Si either during growth, via metalorganic vapor phase epitaxy (MOVPE) [6] [7] [8] [9] or molecular beam epitaxy (MBE) [10] [11], or by implantation and subsequent annealing at high temperature [12] [13]. This latter approach has been demonstrated to be particularly successful, leading to relatively high concentrations of Si shallow donors in AlN [12]. However, the understanding of Si diffusion processes in AlN at elevated temperatures remains limited. These processes are also of interest for epitaxial growth of AlN based heterostructures since the diffusion of Si from the n-doped region into the active region and/or into the p-doped layer at elevated temperature might have detrimental consequences on the device performance.

In this paper, we experimentally study diffusion of Si in bulk AlN to provide key diffusion parameters and to get insights into the defects/defect-complexes

involved in the diffusion process. As a Si source, we use a $Si_{1-x}N_x$ layer deposited by reactive sputtering onto the surface of bulk AlN with low dislocation density (DD < 10^3 cm^{-2}). Diffusion experiments are performed by high temperature annealing at a pressure of 1000 mbar in N_2 environment. The use of high quality AlN bulk substrate allows to neglect diffusion of Si along dislocations and grain boundaries, therefore to investigate the volume diffusion in AlN. Concentration profiles of Si before and after annealing at temperatures between 1500°C and 1700°C, measured by secondary-ion mass spectrometry (SIMS), show a box-like shape. The Si diffusion profiles are best described by Fick's second law of diffusion with a Si diffusion coefficient that depends on the square of the Si concentration. This concentration dependence and the preferred incorporation of Si on the Al lattice site provide strong evidence that Si diffuses via the vacancy mechanism in AlN. Considering theoretical calculations on the formation enthalpy of native point defects in AlN [14] [15], we conclude that Si diffuses via the vacancy mechanism expressed by the reaction $Si_{Al}V_{Al}^{-} + e^{-} \leftrightarrow Si_{Al}^{+1} + V_{Al}^{-3}$, with a single negatively charged dopant-defect pair $Si_{Al}V_{Al}^{-}$ in the foreign-atom controlled diffusion mode. The Si diffusion in AlN is affected by an electric field associated with the incorporation of Si on substitutional Al lattice sites. The impact of an electric field on the Si diffusion indicates a distribution of active Si_{Al}^{+1} donors at the diffusion temperature that is not compensated in the diffusion volume.

SAMPLE PREPARATION AND EXPERIMENTAL METHODS

A freestanding AlN single crystal with low dislocation density (DD < 10^3 cm^{-2}), grown by physical vapor transport via spontaneous nucleation, is sliced into wafers with (0001) orientation using an inner diameter saw [16] [17]. Subsequently, the surface of the AlN wafers is polished using diamond paste with decreasing

grain sizes down to 1 μm and, finally, chemo-mechanical polished using SiO_2 at pH > 10 [18]. A 200 nm thick layer of amorphous $Si_{1-x}N_x$ is deposited on the bulk AlN wafers using reactive sputtering deposition from a Si_3N_4 target with Ar/N_2 gas mixture at $5*10^{-3}$ mbar. The background concentration of Si in the bulk AlN wafers is in the range of 2 to $5*10^{17}$ atoms/cm^3; the concentration of oxygen is in the range of 1 to $4*10^{19}$ atoms/cm^3 and the carbon one between 1 to $2*10^{19}$ atoms/cm^3.

One piece of the bulk AlN with deposited $Si_{1-x}N_x$ is kept as reference, while the other $Si_{1-x}N_x$ deposited bulk AlN wafers, with dimensions of ~1 cm x 1 cm, are annealed in a LORA HTMReetz furnace [19] at a pressure of 1 atm in N_2 ambient. In order to reduce degradation of the $Si_{1-x}N_x$ layer on top of the single crystal AlN bulk sample, an AlN epilayer grown on Al_2O_3 and covered with a 200 nm $Si_{1-x}N_x$ layer is placed face to face with the SiN layer deposited on AlN as shown in fig.1.

FIG. 1. Face to face annealing configuration of bulk AlN with 200 nm $Si_{1-x}N_x$ deposition in interfacial contact with 200 nm $Si_{1-x}N_x$ deposited on an AlN on sapphire structure. This sample configuration serves to protect the $Si_{1-x}N_x$ surface against degradation during high temperature annealing.

Isochronal diffusion anneals for 1 hour (not considering the heating up and cooling down time) are performed at 1500°C, 1600°C and 1700°C as well as isothermal anneals at 1600 °C for 1 h, 2 h and 4 h.

After annealing, Si depth profiles established by diffusion of Si from the top SiN layer into the bulk AlN are measured by SIMS. The analysis of the AlN on sapphire structure used as protective cover is not addressed in this study. SIMS analyses are performed with a Cameca IMS 4f-E6 using 14.5 keV cesium Cs^+ ions and a depth resolution of ~1 nm. The matrix signal $^{27}Al^-$ is taken as reference. Prior to SIMS analysis, a layer of gold with a few nanometers in thickness was sputtered on the surface of the samples in order to reduce charging effects during

the measurements. Implantation standards of carbon, oxygen and silicon in AlN are used for SIMS calibrations. The depth of the craters left from the SIMS measurements were determined by means of a tactile profilometer Rank Taylor Hobson Ltd with a diamond stylus. Using these measurements and considering a constant sputter rate, the depth scale is determined.

RESULTS AND DISCUSSION

Fig. 2 shows SIMS depth profiles of Si in AlN before and after diffusion annealing at the temperatures and times indicated. The dopant profiles recorded after annealing are characterized by a box-like shape with a nearly flat high concentration part close to the interface between $Si_{1-x}N_x$ and AlN and a steep drop in the Si concentration at the diffusion front. The Si concentration beyond the diffusion front reveals the background dopant concentration C_0, which corresponds to the initial concentration of Si in the bulk AlN crystals and is in the range of C_0 =2-5 * 10^{17} at/cm^3.

These Si dopant diffusion profiles are characteristic of a diffusion process with a diffusion coefficient that depends on the local concentration of Si [20]. The Si concentration at the $Si_{1-x}N_x$/AlN interface located at about 200 nm below the surface is considered to reflect the solubility $C_{Si_{Al}^+}^{eq}$ of Si on Al lattice site in AlN obtained under the established experimental conditions.

FIG. 2. Experimental SIMS depth profiles of Si in bulk AlN before and after isothermal annealing at 1600 °C for 1 h, 2 h and 4 h (not considering the heating up and cooling down time) as well as isochronal annealing of 1 h at 1500°C, 1600°C and 1700°C.

The Si concentration profiles $C_{Si_{Al}^+}(x,t)$ are compared to numerical solutions of Fick's second law of diffusion [20]:

$$\frac{\partial C_{Si_{Al}^+}(x,t)}{\partial t} - \frac{\partial}{\partial x} D^{eff}_{Si_{Al}^+}(C_{Si_{Al}^+}(x,t)) \frac{\partial C_{Si_{Al}^+}(x,t)}{\partial x} = 0 \quad (1)$$

with an effective Si diffusion coefficient $D^{eff}_{Si_{Al}^+}(C_{Si_{Al}^+}(x,t))$ that depends on the local Si concentration $C_{Si_{Al}^+}(x,t)$.

Fig. 3 shows numerical solutions of Eq. (1) for different concentration-dependent diffusion coefficients $D^{eff}_{Si_{Al}^+}$ in comparison with the experimental Si profile obtained after diffusion annealing at 1600°C for 1h.

FIG. 3. Experimental Si depth profile measured with SIMS after 1h annealing at 1600°C (black curve) in comparison with diffusion profiles calculated assuming different concentration dependent effective Si diffusion coefficients $D^{eff}_{Si_{Al}^+} \propto (C_{Si_{Al}^+})^n$ with n=0, 1, 2, 3. The best fit is obtained for n=2 (red curve).

In the simulations, the initial Si concentration $C_{Si_{Al}^+}(x > 0, t = 0) = C_0$ is set to the background Si concentration measured by SIMS. The concentration of Si at the $Si_{1-x}N_x$/AlN interface established during diffusion annealing is considered to represent the boundary concentration $C_{Si_{Al}^+}(x = 0, t > 0) = C^{eq}_{Si_{Al}^+}$, i.e., the concentration of the Si_{Al} donor on Al sites under thermal equilibrium.

The reference sample (bulk AlN with $Si_{1-x}N_x$ without thermal treatment) is used to define the position of the $Si_{1-x}N_x$/AlN interface. Fig. 3 reveals that the experimental Si profile measured by SIMS is best described by solutions of Eq. (1) with an effective Si diffusion coefficient $D^{eff}_{Si_{Al}^+}$ that depends on the square of the local Si concentration $C_{Si_{Al}^+}$:

$$D^{eff}_{Si_{Al}^+} = 2D^*_X (C_{Si_{Al}^+})^n \quad (2)$$

with n=2. The parameters D^*_X and $C^{eq}_{Si_{Al}^+}$ are fitted to achieve a good match between experimental (black curve) and simulated profiles. D^*_X describes the concentration independent diffusion coefficient of the mobile defect X. The factor 2 on the right side of Eq. (2) follows from the general mathematical treatment of the diffusion

of mainly substitutionally dissolved dopants in semiconductors whose concentration exceeds the intrinsic carrier concentration at the diffusion temperature. Following this theory of dopant diffusion in semiconductors [20], the diffusion parameter D_X^* reflects the reduced diffusion coefficient of the defect X that mediates the diffusion of Si in AlN (see below).

To evaluate the accuracy of the fit, a comprehensive error analysis is performed, comparing the experimental profiles with the calculated diffusion profiles for the different values of n (n=0, 1, 2, 3). Among these values, the lowest root mean square percentage error (RMSPE) of 22% is achieved for n=2, indicating that the square concentration dependency provides the most favorable fit. It is important to highlight that the main contribution to this error arises from the tails of the profiles at the interfaces of the diffused layer. At these regions, the accuracy of the SIMS measurements may be affected by instrumental broadening due to the abrupt transitions. On the other hand, in the plateau part of the profiles, where measurements are more accurate and better capture the diffusion behavior, a nearly perfect agreement between the experimental and simulated profiles is achieved with n=2. This suggests that the chosen model adequately captures the diffusion behavior within the plateau region, leading to high precision in the results. We conclude that the square concentration dependency (n=2) is the optimal choice for describing the Si profile and yields the most accurate representation of the diffusion process.

Fig. 4 displays the best fits (with n=2) for all the experimental Si concentration profiles assuming a square concentration dependence of the effective diffusion coefficient $D_{Si_{Al}^+}^{eff}$. All Si concentration profiles of both the isochronal and the isothermal annealing series are accurately described. The parameter values for D_X^* and $C_{Si_{Al}^+}^{eq}$ that best reproduce the experimental profiles are listed in Table I.

FIG. 4: Experimental and simulated SIMS concentration profiles of Si in AlN bulk wafers before and after diffusion annealing. (a) Si concentration depth profiles obtained after isochronal anneals at 1500°C, 1600°C and 1700°C for 1 h. (b) Si concentration depth profiles after isothermal anneals at 1600°C for 1 h, 2 h, and 4 h. The dark blue curve represents the SIMS concentration profile of Si before annealing.

The background concentration of Si in the bulk AlN slightly varies for the different samples. This reflects inhomogeneities in the Si concentration in the as-grown crystal and is due to impurities occurring in the source material. These differences are within an acceptable range and do not significantly affect the Si diffusion process, thus the model parameters deduced from fitting the experimental profiles.

Table I. Reduced diffusion coefficient D_X^* and thermal equilibrium concentration $C_{Si_{Al}^+}^{eq}$ determined by fitting the Si concentration profiles in bulk AlN measured by SIMS after diffusion annealing at the temperatures T and times t indicated. Within the framework of the vacancy mechanism, which we consider to mediate the diffusion of Si in AlN, the defect X is the mobile $X = Si_{Al}V_{Al}^-$ defect pair that mediates the formation of the single donor Si_{Al}^{+1} on Al lattice site via a foreign-atom controlled mode of diffusion.

T (°C)	t (h)	10^4/T (K^{-1})	$C_{Si_{Al}^+}^{eq}$ (cm^{-3})	D_X^* (cm^2/s)	$2D_X^*$ (cm^2/s)
1500	1	5.64	3.15 x 10^{19}	6.55 x 10^{-18}	1.31 x 10^{-17}
1600	1	5.34	4.00 x 10^{19}	3.61 x 10^{-17}	7.22 x 10^{-17}
1600	2	5.34	4.50 x 10^{19}	3.47 x 10^{-17}	6.94 x 10^{-17}
1600	4	5.34	5.20 x 10^{19}	4.31 x 10^{-17}	8.61 x 10^{-17}
1700	1	5.07	7.70 x 10^{19}	2.56 x 10^{-16}	5.12 x 10^{-16}

In the literature, few studies on Si diffusion in nitrides are available and they report diffusion parameters under extrinsic doping conditions [13] [21]. So, in order to compare our results with those earlier data, we refer to the extrinsic diffusion coefficient $2D_X^*$ in eq. 2, the values of which are listed in Table I. In the conditions considered in our study, the temperature dependence of the extrinsic diffusion coefficient is described by an Arrhenius behavior with an activation enthalpy of

5.51 ± 0.31 eV and a pre-exponential factor of $0.054\ ^{+0.32}_{-0.05}$ cm^2s^{-1}. This is illustrated by the solid pink line in fig. 5.

FIG. 5: Temperature dependence of the Si diffusion coefficient in AlN for extrinsic conditions determined in this work (solid pink line) in comparison with the results for the Si diffusion coefficient in epitaxial AlN reported by Okomura et al. [13] (blue line) and for the Si diffusion coefficient in epitaxial GaN by Jakiela et al. [21] (yellow line).

In addition, fig. 5 shows the comparison of our results on Si diffusion in AlN under the considered extrinsic experimental conditions with the data presented by Okomura et al. [13] in their study on impurity diffusion in AlN and with those by Jakiela et al. [21] on Si diffusion in GaN. It has to be considered that those earlier studies were performed on nitride layers on sapphire substrates, where the contribution of dislocations to the diffusion process cannot be excluded. In contrast, we use high-quality bulk AlN that allows to neglect Si diffusion along dislocations.

Concerning Si diffusion in AlN on sapphire, Okomura et al. [13] report a pre-exponential factor of 4×10^{-10} cm^2s^{-1} and an activation enthalpy of 1.35 eV. While for Si diffusion in epitaxial GaN on sapphire, Jakiela et al. [21] calculated a value of 9.1×10^{-8} cm^2s^{-1} for the pre-exponential factor and 1.55 eV for the activation enthalpy. These values are significantly lower compared to the ones determined in the context of our study. Okomura et al. [13] performed diffusion experiments on Si-implanted AlN layers on sapphire using thermal annealing. They assumed a finite source of Si and a constant diffusion coefficient, obtaining a partially good fit of the experimental Si depth profiles only for the region at high Si concentration (i.e. $>10^{19}$ cm^{-3}). On the other hand, in our study, considering an infinite source of Si and a diffusion coefficient dependent on the square of the local Si concentration, we are able to obtain a very good fit for the whole experimental Si box-shape profiles, as shown in fig. 4 and, accordingly, we consider our diffusion data to be more meaningful.

The Si diffusion profiles alone do not provide direct evidence of the defects responsible for mediating the diffusion process in AlN. However, some insights on the mechanism of Si diffusion in AlN can be drawn from the shape of the Si profile, from the preferred incorporation of Si on the substitutional Al lattice site of AlN and from the nature of the native point defects in AlN which are favored under nitrogen-rich conditions. The distinctive box-shaped dopant profile with a steep front is typically associated with strong extrinsic conditions prevailing during the diffusion process. Such a profile provides clear indications of n-type doping conditions, implying that Si exhibits high electrical activity at the diffusion temperatures. Theoretical studies have shown that Al and N vacancies are the dominant intrinsic defects in wurtzite AlN. Density functional theory (DFT) calculations have revealed that Al vacancies and their complexes with Si or oxygen (O) are energetically favored when the Fermi level (E_F) is close to the conduction band, i.e., at high n-type doping conditions [14] [15] [22]. Among the predicted native defects under these conditions, triply negatively charged vacancies on the Al site (V_{Al}^{-3}) are considered to be the most favored under nitrogen-rich conditions [14]. Based on these considerations, it is plausible to conclude that the diffusion of Si in AlN is mediated by a vacancy mechanism that involves the formation of complexes between the singly positively charged Si donors on substitutional Al sites $\left(Si_{Al}^{+1}\right)$ and the triple negatively charged Al vacancies (V_{Al}^{-3}). This is expressed by the reaction:

$$Si_{Al}V_{Al}^{-} + e^{-} \leftrightarrow Si_{Al}^{+1} + V_{Al}^{-3} \quad (3)$$

where $Si_{Al}V_{Al}^{-}$ is a singly negatively charged dopant-defect pair representing the mobile species mediating the diffusion process and e^- an electron to keep the charge balance of the defect reaction [20]. The interface between the amorphous SiN layer and the AlN is considered to be the main source for vacancies during the diffusion process. Following the general analysis of dopant diffusion in semiconductors reported by Bracht [20], the formation of the immobile Si_{Al}^{+1} defect

on the Al sublattice (as reported in eq. 3) can be controlled either by the diffusion of the mobile $Si_{Al}V_{Al}^{-}$ defect pair or by the diffusion of the vacancy V_{Al}^{-3}. In the former scenario, the effective diffusion ($D_{Si_{Al}^{+}}^{eff}$) proceeds in a foreign-atom controlled mode, while in the latter case, in a native-defect controlled mode of diffusion. The native-defect controlled diffusion of Si via vacancy mechanism would suggest a concentration-independent effective diffusion coefficient $D_{Si_{Al}^{+}}^{eff}$ (see Eq. (42) in reference [20]). This contradicts our observed experimental results, which clearly demonstrate that Si diffusion in AlN is proportional to the square of the Si concentration (Eq. (2)). On the other hand, the foreign-atom controlled mode of Si diffusion via the vacancy mechanism predicts a square dependence of the effective Si diffusion $D_{Si_{Al}^{+}}^{eff}$ on the Si concentration (see Eq. (47) in reference [20]). This is in accurate agreement with our experimental results. So, we conclude that Si diffusion in AlN proceeds in the foreign-atom controlled diffusion mode and the mobile species governing this diffusion process is the singly negatively charged defect pair $Si_{Al}V_{Al}^{-}$.

The characteristic box-shaped Si profile indicates that Si diffusion is strongly affected by the electric field resulting from Si incorporation on substitutional Al lattice sites Si_{Al}^{+1}. This profile shape is not expected in case of strong compensation of the donor dopant Si_{Al}^{+1} during the diffusion process [20]. The general case of dopant diffusion in semiconductors through the vacancy mechanism is described by a system of coupled partial-differential equations accounting for each point defect potentially involved in the diffusion process [20]. However, in specific situations where the donor concentration is high (exceeding the intrinsic concentration), the free carrier concentration approximately matches the concentration of donors. This allows to simplify the set of coupled partial-differential equations into a single differential equation (expressed by equation 1), which effectively describes Si diffusion in AlN under consideration in this study.

Accordingly, we can conclude that the free carrier concentration at the diffusion temperature is nearly equal to the concentration of Si donors on Al sites, which remain fully electrically active during high-temperature diffusion.

Table I reports the values determined for the reduced diffusion coefficient D_X^* with $X = Si_{Al}V_{Al}^-$. These values are representative for the doping conditions realized in the diffusion experiments. Under different extrinsic doping conditions also different values of $D^*_{Si_{Al}V_{Al}^-}$ are expected. Accordingly, extrinsic doping conditions are not an appropriate reference for $D^*_{Si_{Al}V_{Al}^-}$. Commonly, diffusion data obtained for extrinsic conditions are converted to intrinsic doping conditions as reference state. This is essential to establish a baseline for comparing Si diffusion data determined under various doping conditions. In the following, the extrinsic data for $D^*_{Si_{Al}V_{Al}^-}$ are converted to intrinsic conditions.

In this context, first the physical meaning of the reduced diffusion coefficient $D^*_{Si_{Al}V_{Al}^-}$ must be clarified. In the framework of the vacancy mechanism in reaction (3), $D^*_{Si_{Al}V_{Al}^-}$ is given by [20]:

$$D^*_{Si_{Al}V_{Al}^-} = \frac{\left(C^{eq}_{Si_{Al}V_{Al}^-}\right)\left(D_{Si_{Al}V_{Al}^-}\right)}{C^{eq}_{Si_{Al}^+}} \tag{4}$$

where $C^{eq}_{Si_{Al}V_{Al}^-}$ and $D_{Si_{Al}V_{Al}^-}$ are the thermal equilibrium concentration and diffusion coefficient of the singly negatively charged dopant-defect pair $Si_{Al}V_{Al}^-$, respectively. $C^{eq}_{Si_{Al}^+}$ is the equilibrium concentration of the singly positively charged Si atoms on Al lattice sites. Considering the impact of doping on the formation of charged defects, their equilibrium concentration depends on the position of the Fermi level, i.e., with increasing n-type doping the Fermi level shifts to the conduction band and, as a consequence, $C^{eq}_{Si_{Al}V_{Al}^-}$ increases and $C^{eq}_{Si_{Al}^+}$ decreases. This is generally expressed by the ratio [20]

$$\frac{C_{X^z}^{eq}}{C_{X^z}^{eq,in}} = \left(\frac{n_{in}}{n^{eq}}\right)^z \tag{5}$$

between the equilibrium concentrations of the defect X^z with charge state $z \in \{\pm 1, \pm 2, \dots\}$. $C_{X^z}^{eq,in}$ and $C_{X^z}^{eq}$ are the equilibrium concentrations of X^z under intrinsic and extrinsic doping conditions, respectively; n_{in} represents the intrinsic carrier concentration and n^{eq} is the maximum free electron concentration calculated via the neutrality equation for the maximum dopant concentration in the semiconductor (see Eq. (34) in reference [20]). By means of Eq. (5), $D^*_{Si_{Al}V_{Al}^-}$ for extrinsic conditions can be converted to $D^*_{Si_{Al}V_{Al}^-}(n_{in})$ for intrinsic conditions:

$$D^*_{Si_{Al}V_{Al}^-}(n_{in}) = D^*_{Si_{Al}V_{Al}^-}\left(\frac{n_{in}}{n^{eq}}\right)^2 \tag{6}$$

where n^{eq} is approximated by $n^{eq} \approx C_{Si_{Al}^+}^{eq}$ for the respective temperatures. The intrinsic carrier concentration n_{in} is given by [23] [24]

$$n_{in}^2 = N_v N_c \exp\left(-\frac{E_g}{k_B T}\right) \tag{7}$$

where E_g, N_v, and N_c represent, respectively, the energy bandgap, the density of states in the valence and conduction band. For the temperature dependence of these parameters, we consider the following expressions [25]:

$$N_v(T) = N_v(300K)\left(\frac{T}{300K}\right)^{3/2} \tag{8}$$

$$N_c(T) = N_c(300K)\left(\frac{T}{300K}\right)^{3/2} \tag{9}$$

$$E_g(T) = E_g(0K) - 1.799 * 10^{-3}\left(\frac{T^2}{T + 1462}\right) \tag{10}$$

with $N_v(300K) = 4.9 * 10^{20}\ cm^{-3}$, $N_c(300K) = 6.2 * 10^{18}\ cm^{-3}$ and $E_g(0K) = 6.2\ eV$ [24] [26] [27]. The calculated values for n_{in} are given in Table II for the respective diffusion temperatures.

Table II. Densities of states in the conduction band N_c and valence band N_v, the energy bandgap E_g and the intrinsic carrier concentration n_{in} in AlN at the temperatures T indicated.

T (°C)	10^4/T (K^{-1})	N_c (cm^{-3})	N_v (cm^{-3})	E_g (eV)	n_{in} (cm^{-3})
1500	5.64	8.90×10^{19}	7.04×10^{21}	4.45	3.74×10^{14}
1600	5.34	9.67×10^{19}	7.64×10^{21}	4.31	1.38×10^{15}
1700	5.07	1.05×10^{20}	8.26×10^{21}	4.16	4.52×10^{15}

By means of Eq. (6) and the data calculated for n_{in} listed in Table II, the reduced diffusion coefficient $D^*_{Si_{Al}V_{Al}^-}(n_{in})$ for intrinsic conditions is obtained. The data are given in Table III for the respective temperatures and shown in fig. 6 as function of the inverse temperature. The temperature dependence of $D^*_{Si_{Al}V_{Al}^-}(n_{in})$ is described by the Arrhenius equation:

$$D = D_0 \exp\left(-\frac{E_A}{k_B T}\right) \tag{11}$$

where k_B is the Boltzmann's constant, while D_0 and E_A are the pre-exponential factor and the activation enthalpy of diffusion, respectively.

FIG. 6. The reduced diffusion coefficient $D^*_{Si_{Al}V_{Al}^-}(n_{in})$ for intrinsic doping conditions as function of the inverse temperature 10^4/T. The temperature dependence is described by an Arrhenius equation with an activation enthalpy of (10.34 ± 0.32) eV and a pre-exponential factor of $235\ ^{+1485}_{-203}$ cm^2s^{-1}.

The temperature dependence of $D^*_{Si_{Al}V_{Al}^-}(n_{in})$ is best described by an activation enthalpy $E_{A,1} = 10.34 \pm 0.32$ eV and a pre-factor $D_{0,1} = 235\ ^{+1485}_{-203}$ cm^2s^{-1}.

Table III. Reduced diffusion coefficient D^*_X for intrinsic doping conditions at the temperatures T and times t indicated. Transport capacity of the mobile dopant-vacancy in extrinsic and intrinsic doping conditions, both normalized to the atom density $C_{Al} = 4.78 * 10^{22}$ of Al.

T (°C)	t (h)	$D^*_{Si_{Al}V_{Al}^-}(n_{in})$ (cm^2/s)	$C^{eq}_{(Si_{Al}V_{Al}^-)}D_{(Si_{Al}V_{Al}^-)}/C_{Al}$ (cm^2/s)	$C^{eq}_{(Si_{Al}V_{Al}^-)}(n_{in})D_{(Si_{Al}V_{Al}^-)}/C_{Al}$ (cm^2/s)
1500	1	9.26×10^{-28}	4.32×10^{-21}	5.13×10^{-26}

1600	1	4.32 x 10^{-26}	3.02 x 10^{-20}	1.04 x 10^{-24}
1600	2	3.28 x 10^{-26}	3.27 x 10^{-20}	1.00 x 10^{-24}
1600	4	3.05 x 10^{-26}	4.68 x 10^{-20}	1.25 x 10^{-24}
1700	1	8.82 x 10^{-25}	4.12 x 10^{-19}	2.42 x 10^{-23}

By rearranging Equation (4), the transport capacity of the mobile dopant-vacancy pair is given by the product:

$$C^{eq}_{Si_{Al}^{+}} D^{*}_{Si_{Al}V_{Al}^{-}} = C^{eq}_{(Si_{Al}V_{Al}^{-})} D_{(Si_{Al}V_{Al}^{-})} \quad (12)$$

The data thus obtained represent the values of the transport capacity for extrinsic doping conditions. The corresponding values are normalized to the atom density $C_{Al} = 4.78 * 10^{22}\ cm^{-3}$ of Al and listed in Table III in units of cm^2/s.

The transport capacity for intrinsic conditions is given by

$$C^{eq}_{(Si_{Al}V_{Al}^{-})}(n_{in}) D_{(Si_{Al}V_{Al}^{-})} = C^{eq}_{(Si_{Al}V_{Al}^{-})} D_{(Si_{Al}V_{Al}^{-})} \frac{n_{in}}{n^{eq}} \quad (13)$$

The values obtained are listed in Table III and, also in this case, they are normalized to the atom density C_{Al}.

FIG. 7: Temperature dependence of the transport capacity $C^{eq}_{(Si_{Al}V_{Al}^{-})}(n_{in}) D_{(Si_{Al}V_{Al}^{-})}/C_{Al}$ deduced from the analysis of Si diffusion in AlN. The temperature dependence is best described by an Arrhenius equation with an activation enthalpy $E_{A,2} = 9.26 \pm 0.32$ eV and a pre-exponential factor $D_{0,2} = 9.9\ ^{+61.0}_{-8.5}\ cm^2 s^{-1}$ of the mobile defect $Si_{Al}V_{Al}^{-}$.

The temperature dependence of the transport capacity $\left(C^{eq}_{(Si_{Al}V_{Al}^{-})}(n_{in}) D_{(Si_{Al}V_{Al}^{-})}/C_{Al}\right)$ is accurately described by an Arrhenius equation with an activation enthalpy $E_{A,2} = 9.26 \pm 0.32$ eV and a pre-exponential factor $D_{0,2} = 9.9\ ^{+61.0}_{-8.5}\ cm^2 s^{-1}$ of the mobile defect $Si_{Al}V_{Al}^{-}$. This is illustrated in fig. 7 by the black solid line.

The activation enthalpy of the transport capacity, being the latter defined as the product of the equilibrium concentrations and diffusion coefficient of the mobile defect $Si_{Al}V_{Al}^{-}$, represents the sum of its formation and migration enthalpy. Harris

et al. [3] report theoretical calculations for the formation energy of the $Si_{Al}V_{Al}$ defect complex in its various charge states. For n-type doping conditions, i.e., the Fermi level is in the upper half of the band gap, Harris et al. predict that the doubly negatively charged complex $\left(Si_{Al}{V_{Al}}^{2-}\right)$ is the most stable among the other $Si_{Al}V_{Al}$ complexes with different charge states, with a formation energy below 2 eV for Si-rich conditions [3]. For intrinsic conditions, i.e., the Fermi level is in the mid gap position, the formation energy of $Si_{Al}{V_{Al}}^{2-}$ increases to a value of about 5.3 eV and the formation energy of $Si_{Al}{V_{Al}}^{-}$ is estimated to be about 5.8 eV (see fig. 3 in reference [3]). Compared to these theoretical calculations supporting the dominance of the double negatively charge state of the $Si_{Al}V_{Al}$ complex under high n-type doping, the Si diffusion experiments reported in our study reveal that the $Si_{Al}V_{Al}$ complex is singly negatively charged at the considered diffusion temperatures. This disparity does not disprove the theoretical calculations by Harris et al. [3], whose formation energies are representative for $T = 0$ K, but it rather shows that a direct comparison with theoretical calculations is difficult as the band gap shrinks with increasing temperature. As a result, also the formation of complexes between vacancies and Si atoms on the Al sites is expected to be dependent on the temperature. Neglecting this temperature dependence for simplicity and assuming an energy of 5.8 eV for the formation of the $Si_{Al}{V_{Al}}^{-}$ under electronically intrinsic conditions, an energy of about 3.5 eV is obtained for the migration of the donor-vacancy complex $Si_{Al}{V_{Al}}^{-}$. Considering that the Si atom in Si-vacancy complexes in AlN occupies an Al second nearest neighbor site to the Al vacancy, the migration of the defect complex can involve both first and second nearest neighbor jumps and the formation of anti-site defects. Thus, a migration energy of several eV for the donor-vacancy complex $Si_{Al}{V_{Al}}^{-}$ is considered to be realistic.

CONCLUSIONS

This study provides fundamental parameters for the diffusion of Si donors in AlN. We investigated Si diffusion in bulk AlN with DD < 10^3 cm^{-2} and obtained concentration profiles that are best described with a diffusion coefficient dependent on the square of the local Si concentration. This specific diffusion behavior of Si in AlN is explained on the basis of the vacancy mechanism. By analyzing the experimental SIMS depth profiles, we determined the parameters governing the diffusion of Si in AlN under the specific extrinsic experimental conditions and we compared our results with the existing data provided in the literature. Subsequently, we converted our diffusion data for extrinsic doping to intrinsic doping conditions as reference state. The linear dependence of the reduced diffusion coefficient for the intrinsic conditions on the reciprocal temperature provided the value of the activation enthalpy $E_{A,1} = 10.34 \pm 0.32\,eV$ under these intrinsic conditions. Furthermore, considering that the diffusion of Si in AlN proceeds in the foreign-atom-controlled mode of the vacancy mechanism, we identified the dopant-defect pair ($Si_{Al}V_{Al}^{-}$) as the mobile species governing the diffusion process. Exploiting the linear behavior of the transport capacity of $Si_{Al}V_{Al}^{-}$ with the reciprocal temperature and considering theoretical DFT calculations from previous studies on highly n-doped AlN, the migration enthalpy of the mobile donor-vacancy complex $Si_{Al}V_{Al}^{-}$ was estimated to be around 3.5 eV under intrinsic conditions. The Si diffusion in AlN is shown to be affected by the electric field associated with the incorporation of Si on substitutional Al lattice sites. The characteristic box-like Si profile reflects the distribution of active Si_{Al}^{+1} donors in the diffusion volume electrically active at the diffusion temperature. On the other hand, previous studies on Si in AlN have shown significant deactivation at room temperature [3] [4] [5] [8]. This suggests that the deactivation does not occur during the diffusion process at elevated temperature but rather during the cooling phase from high temperature to room temperature. A comparison of the Si diffusion profiles with electrical

measurements at room temperature with nanometer resolution would help to asses the local degree of compensation [28]. This would contribute to identify the physical origin of the Si compensation, leading to a more comprehensive understanding of Si behavior in AlN and its applications. This study could potentially open new perspectives for n-type doping in AlN by Si diffusion.

ACKNOWLEDGEMENTS

This work was partially supported by the French Program GaNeX, "Investissements d'Avenir".

The authors would like to thank Dr. Ina Ostermay from FBH for assistance with the $Si_{1-x}N_x$ deposition. Part of the work was supported by the German Federal Ministry of Education and Research (BMBF) within the Advanced UV for Life project (No. 03ZZ0134B).

AUTHOR DECLARATIONS

Conflict of Interest

The authors have no conflicts to disclose.

DATA AVAILABILITY

The data that support the findings of this study are available from the corresponding author upon reasonable request.

REFERENCES

[1]S. B. Zhang, S.-H. Wei and A. Zunger, Phys. Rev. Lett. 84, 1232 (2000). https://doi.org/10.1103/PhysRevLett.84.1232

[2]J.Y. Tsao et al., Adv. Electron. Mater. 4, 1600501 (2018). https://doi.org/10.1002/aelm.201600501

[3]J. S. Harris, J. N. Baker, B. E. Gaddy, I. Bryan, Z. Bryan, K. J. Mirrielees, P. Reddy, R. Collazo, Z. Sitar and D. L. Irving, Appl. Phys. Lett. 112, 152101 (2018). https://doi.org/10.1063/1.5022794

[4]C. G. Van de Walle, Phys. Rev. B 57, R2033(R) (1998). https://doi.org/10.1103/PhysRevB.57.R2033

[5]F. Mehnke, X. T. Trinh, H. Pingel, T. Wernicke, E. Janzén, N. T. Son, and M. Kneissl, Journal of Applied Physics 120, 145702 (2016). https://doi.org/10.1063/1.4964442

[6]Y. Shimahara, H. Miyake, K. Hiramatsu, F. Fukuyo, T. Okada, H. Takaoka and H. Yoshida, Jpn. J. Appl. Phys. 50 095502 (2011). https://doi.org/10.1143/JJAP.50.095502

[7]Y. Taniyasu, M. Kasu, and N. Kobayashi, Appl. Phys. Lett. 81, 1255 (2002). https://doi.org/10.1063/1.1499738

[8]I. Bryan, Z. Bryan, S. Washiyama, P. Reddy, B. E. Gaddy, B. Sarkar, M. H. Breckenridge, Q. Guo, M. B. Graziano, J. Tweedie, S. Mita, D. L. Irving, R. Collazo, and Z. Sitar, Appl. Phys. Lett. **112**, 062102 (2018). https://doi.org/10.1063/1.5011984

[9]M.D. Bremser, W.G. Perry, T. Zheleva et al., MRS Internet Journal of Nitride Semiconductor Research **1**, 8 (1996). https://doi.org/10.1557/S1092578300001800

[10]D. Korakakis, H.M. Ng, K.F. Ludwig et al., MRS Online Proceedings Library 449, 233–238 (1996). https://doi.org/10.1557/PROC-449-233

[11]E. Calleja, M. A. Sánchez-García, E. Monroy, F. J. Sánchez and E. Muñoz, Journal of Applied Physics 82, 4681-4683 (1997). https://doi.org/10.1063/1.372052

[12]M. H. Breckenridge, P. Bagheri, Q. Guo, B. Sarkar, D. Khachariya, S. Pavlidis, J. Tweedie, R. Kirste, S. Mita, P. Reddy, R. Collazo and Z. Sitar, Appl. Phys. Lett. 118, 112104 (2021). https://doi.org/10.1063/5.0042857

[13]H. Okumura, Y. Watanabe, T. Shibata, K. Yoshizawa, A. Uedono, H. Tokunaga, S. Koseki, T. Arimura, S. Suihkonen and T. Palacios, Japanese Journal of Applied Physics 61, 026501 (2022). https://doi.org/10.35848/1347-4065/ac47aa

[14]C. Stampfl et al., Phys. Rev. B 65, 155212 (2002). https://doi.org/10.1103/PhysRevB.65.155212

[15]Q. Yan, A. Janotti, M. Scheffler and C. G. Van de Walle, Appl. Phys. Lett. 105, 111104 (2014). https://doi.org/10.1063/1.4895786

[16]C. Hartmann, J. Wollweber, A. Dittmar, K. Irmscher, A. Kwasniewski, F. Langhans, T. Neugut and M. Bickermann, Jpn. J. Appl. Phys. 52, 08JA06 (2013). http://doi.org/10.7567/JJAP.52.08JA06

[17]C. Hartmann, A. Dittmar, J. Wollweber and M. Bickermann, Semiconductor Science and Technology 29 (8), 084002 (2014). http://doi.org/10.1088/0268-1242/29/8/084002

[18]X. F. Chen, D. Siche, M. Albrecht, C. Hartmann, J. Wollweber and X. G. Xu, Crystal Research and Technology 43 (6), 651-655 (2008). https://doi.org/10.1002/crat.200800057

[19]S. Hagedorn, A. Mogilatenko, S. Walde, D. Pacak, J. Weinrich, C. Hartmann, M. Weyers, Phys. Status Solidi B 2021, 258, 2100187. https://doi.org/10.1002/pssb.202100187

[20]H. Bracht, Phys. Rev. B 75, 035210 (2007). https://doi.org/10.1103/PhysRevB.75.035210

[21]R. Jakieła, A. Barcz, E. Dumiszewska and A. Jagoda, physica status solidi (c). 3. 1416 – 1419 (2016). https://doi.org/10.1002/pssc.200565112

[22]W. Shockley and J. L. Moll, Phys. Rev. 119, 1480 (1960). https://doi.org/10.1103/PhysRev.119.1480

[23]H. Mehrer, *Diffusion in solids*, 1st ed. (Springer Berlin, Heidelberg, 2010).

[24]E.F. Shubert, *Physical Foundations of Solid-State Devices* (New York, 2015).

[25]B. Van Zeghbroeck, *Principles of Semiconductor Devices* (Prentice Hall, New York, 2008).

[26]Q. Guo and A. Yoshida, Jpn. J. Appl. Phys. 33, part 1, 5A (1994), 2453-2456. https://doi.org/10.1143/JJAP.33.2453

[27]H. Teisseyre, P. Perlin, T. Suski, I. Grzegory, S. Porowski, J. Jun, A. Pietraszko and T.D. Moustakas, Journal of Applied Physics 76, 2429 (1994). https://doi.org/10.1063/1.357592

[28]J. K. Prüßing, G. Hamdana, D. Bougeard, E. Peiner and H. Bracht, J. Appl. Phys. 125, 085105 (2019). https://doi.org/10.1063/1.5066617

PLEASE CITE THIS ARTICLE AS DOI: 10.1063/5.0159641

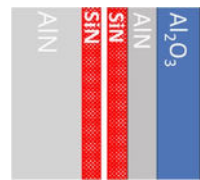

AIP Publishing

Journal of Applied Physics

ACCEPTED MANUSCRIPT

PLEASE CITE THIS ARTICLE AS DOI: 10.1063/5.0159641

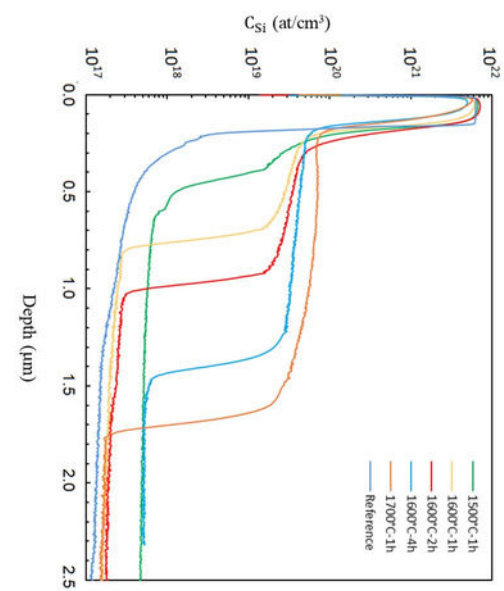

AIP Publishing

Journal of Applied Physics

ACCEPTED MANUSCRIPT

PLEASE CITE THIS ARTICLE AS DOI: 10.1063/5.0159641

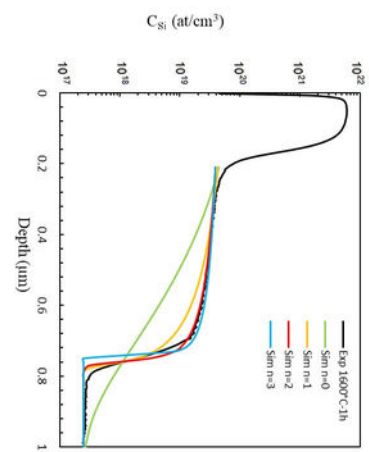

AIP Publishing

Journal of Applied Physics

PLEASE CITE THIS ARTICLE AS DOI: 10.1063/5.0159641

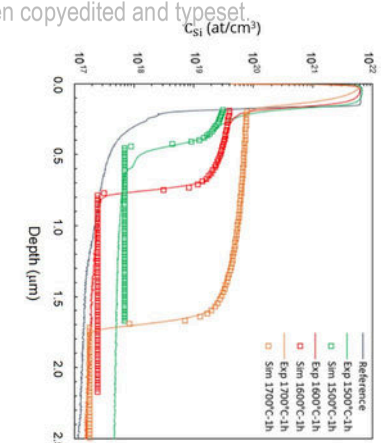

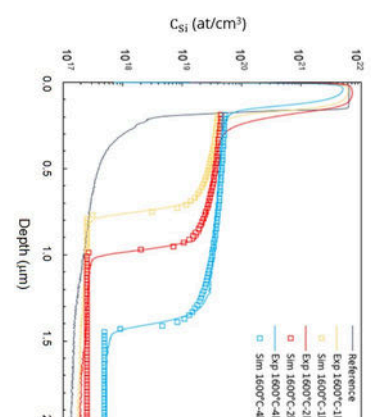

AIP Publishing

Journal of Applied Physics

ACCEPTED MANUSCRIPT

PLEASE CITE THIS ARTICLE AS DOI: 10.1063/5.0159641

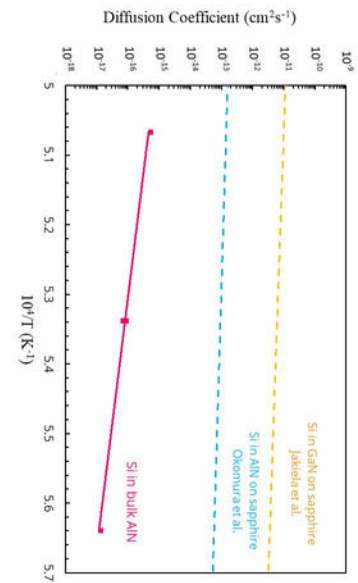

AIP Publishing

Journal of Applied Physics

ACCEPTED MANUSCRIPT

PLEASE CITE THIS ARTICLE AS DOI: 10.1063/5.0159641

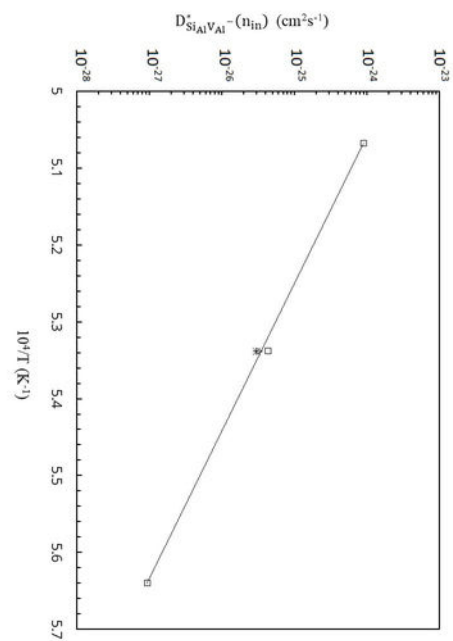

AIP Publishing

Journal of Applied Physics

PLEASE CITE THIS ARTICLE AS DOI: 10.1063/5.0159641